

Young stellar clusters and H₂ nebulosities in S233IR^{*,**}

A. Porras¹, I. Cruz-González², and L. Salas³

¹ Instituto Nacional de Astrofísica, Óptica y Electrónica, Apartado Postal 216, Puebla, Pue. 72000, México (aporras@inaoep.mx)

² Instituto de Astronomía, UNAM, Apartado Postal 70-264, C.U., México, D.F. 04510, México (irene@astroscu.unam.mx)

³ Instituto de Astronomía, UNAM, Apartado Postal 877, Ensenada, B.C. 22830, México (salas@astroscu.unam.mx)

Received 11 January 2000 / Accepted 30 June 2000

Abstract. We present an infrared photometric study of the star formation region associated to IRAS 05358+3543, hereafter designated S233IR. Several manifestations of star formation activity are present in S233IR: masers, molecular outflow, GMC core, YSOs, young stellar clusters and an IRAS source. The paper includes photometric J, H, K and H₂ (2.12 μm) images and scanning Fabry-Perot observations to study H₂ kinematics. In the 3.6' × 3.6' observed field, two distinct young stellar clusters separated by 0.5 pc are found, one being much redder than the other by $A_V \sim 7$ mag. A collection of PMS objects and several H₂ nebulosities associated to the younger and redder NE cluster are found. Two deeply embedded jet/counter-jet structures, produced by shocked H₂ gas, are detected near the core of the molecular outflow. Possible exciting source candidates of the molecular outflow and H₂ nebula are discussed. The velocity field of H₂ gas shows that the bulk of the emission occurs within -36.9 to 2.3 km/s. Individual spectra of H₂ nebulosities show peak velocities consistent with the rest velocity of the GMC and H₂O maser peak velocities. Luminosity function histograms are used to obtain a crude age estimate for cluster and field stars: $\lesssim 2$ Myr for NE cluster, 3 Myr for SW cluster and 6 Myr for field (distributed population) stars; indicating at least two star formation stages and a distributed population of young stars. Finally, from PMS isochrones and NIR photometry, taking care of completeness limits, we estimate stellar masses to study the IMF. A turnover for low-mass-stars is found for the SW cluster, while field stars show a Salpeter IMF.

Key words: stars: early-type – stars: formation – stars: mass-loss – ISM: individual objects: S233IR – ISM: jets and outflows

1. Introduction

We have been studying in the NIR young stellar clusters (YSCs) near HII regions and IRAS sources located along the Perseus

Send offprint requests to: I. Cruz-González

* Based on observations obtained at the Observatorio Astronómico Nacional at San Pedro Mártir, B.C., México.

** Table 1 is only available in electronic form at the CDS via anonymous ftp to cdsarc.u-strasbg.fr (130.79.128.5) or via http://cdsweb.u-strasbg.fr/Abstract.html

Correspondence to: irene@astroscu.unam.mx

Arm. Our aim is to derive extinction to individual stars, luminosity functions, cluster ages and individual stellar masses, with the main goal of studying the stellar mass distribution (IMF) of 45 YSCs in Perseus (Porras et al. 2000). In order to describe our methodology and analysis we present here the study of an embedded SFR near S233, hereafter designated S233IR. We selected this region for a detailed study because it also contains H₂ nebulosities that resemble Herbig-Haro objects, as some of the regions in our Perseus survey (e.g. S187IR, Salas et al. 1998).

We observed the region surrounding the IRAS source 05358+3543 ($\alpha_{1950} = 05^h 35^m 48.8^s$, $\delta_{1950} = +35^\circ 43' 41''$), which has been associated to the HII region S233 (e.g. Chan et al. 1996; Henning et al. 1992) based on its position by Israel & Felli (1978). As is shown in Fig. 1, S233 is part of a giant molecular cloud that includes four HII regions: S231, S232, S233, S235, with S233 being the smallest and closer to IRAS 05358+3543. The association of the IRAS source and the HII regions is supported by CO maps of the GMC by Heyer et al. (1996) over an area of $\sim 3^\circ \times 2^\circ$ in the sky. A maximum peak of $V_{LSR} \sim -17$ km/s from the spatially averaged spectra over the entire region is detected, which agrees with previous observations by Snell et al. (1990) for a region of $6' \times 6'$ centered on the IRAS source.

We adopt a conservative value of 1.8 kpc to the IRAS source and its associated star forming region. From the spectral type of the HII regions exciting source, values of 1.6 ± 0.50 kpc for S235, 2.3 ± 0.7 kpc for S231 (Fich & Blitz 1984) and 2.3 ± 0.7 kpc for S233 (Chan & Fich 1995), have been reported. Nevertheless, the 1.8 kpc value (Evans & Blair 1981) has been widely used (e.g. Wilking et al. 1989; Snell et al. 1990; Henning et al. 1992; Hodapp 1994; Schreyer et al. 1996), since it represents a mean spectroscopic distance value to S235.

IRAS 05358+3543 is a candidate for a star forming region according to several criteria (e.g. Wood & Churchwell 1989; Hughes & MacLeod 1989; Palagi et al. 1993) based on the IRAS observed fluxes. This is supported by maser detections in the region (see Fig. 1). VLA observations of H₂O maser by Tofani et al. (1995) with 0.1'' position accuracy, show four emission peaks located to the NE of IRAS 05358+3543. Also, an OH maser detected by Wouterloot et al. 1988 (30'' position accuracy) located to the NE of H₂O masers; while methanol maser emission observed by Menten (1991) (HPBW = 5') lies closer to the H₂O masers.

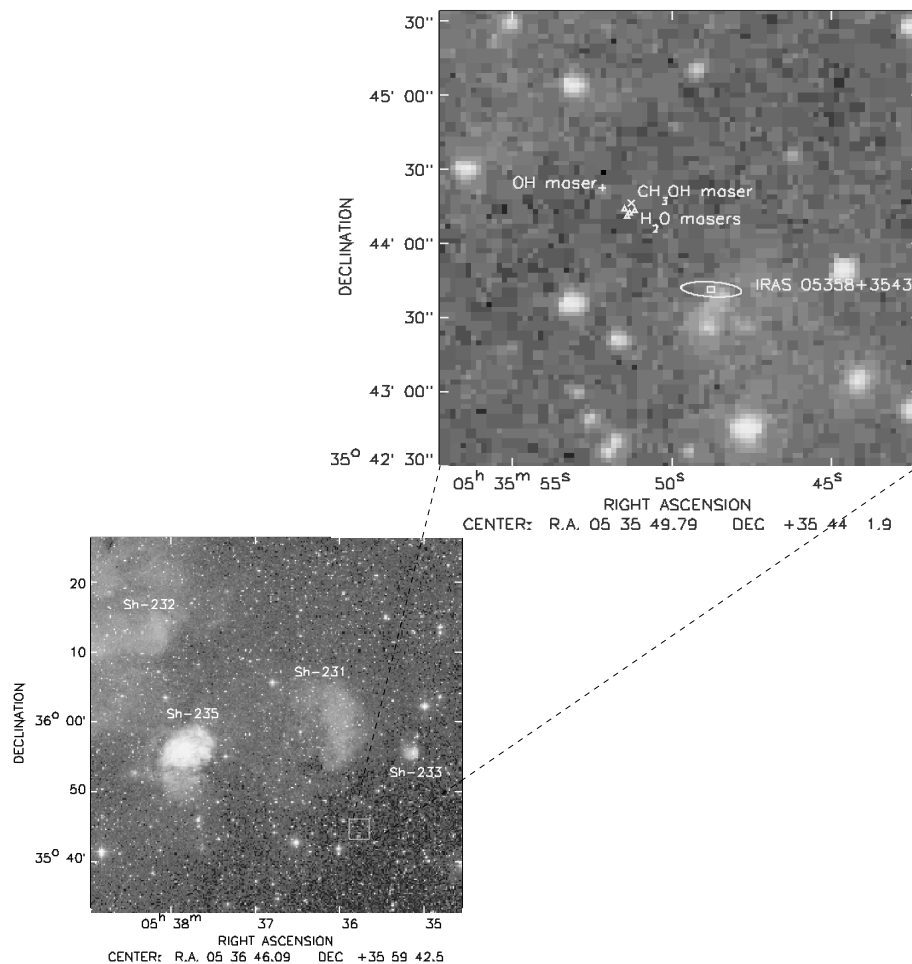


Fig. 1. Optical maps from the complex of Sharpless H II regions (from left to right) S232, S235, S231 and S233. The enlargement of the observed region includes the location of IRAS 05358+3543 with its error ellipse, and the positions of H₂O (Δ), OH (+) and CH₃OH (×) maser detections (Tofani et al. 1995; Wouterloot et al. 1988; Menten 1991).

Different observations of molecular lines in S233IR have been reported and show that the associated region is a core source in the GMC (e.g. ¹³CO detected by Casoli et al. 1986 and Wilking et al. 1989; ¹²CO by Wouterloot & Brand 1989; CS (2-1) by Bronfman et al. 1996; HCO⁺ (1-0) by Richards et al. 1987 and Schreyer et al. 1996; NH₃ (1,1) and (2,2) by Schreyer et al. 1996. Casoli et al. 1986 estimated that the GMC associated with S231, S233 and S235 has a gas column density $N_{H_2} = 55 \times 10^{20} \text{ cm}^{-2}$ and mass $M_{H_2} = 450 M_{\odot}$.

S233IR was observed at K' (7' × 3' field) by Hodapp (1994), with limiting magnitude 17.5. He notes the presence of an embedded young stellar cluster, two bright stars with associated nebulosity and nebular features probably excited by shocks that resemble HH objects. However, Wilking et al. (1989) failed to detect mm continuum sources in the region.

Several star formation tracers are found in S233IR: masers, molecular outflows, high density cores, stellar clusters and an IRAS source, making it an excellent candidate for a near-IR study. In this paper we present JHK photometric observations (Sect. 2 and Sect. 3) and a study of molecular hydrogen emission (Sect. 4). Several infrared H₂ nebulosities are detected with characteristics of shock features. Velocity maps of H₂ gas are studied via Fabry-Perot observations and compared to kinematic radio studies. Possible exciting sources of these H₂ nebulosi-

ties, fluxes, morphology and velocities suggest that S233IR contains two jet/counter-jet deeply embedded Herbig-Haro objects (Sect. 5). We show that S233IR is a singular example of two young embedded clusters at a different evolutionary state. The luminosity function and IMF of cluster and distributed population stars are addressed (Sect. 5).

2. Observations

2.1. Direct imaging

Observations were obtained with the IR camera CAMILA (Cruz-González et al. 1994) at the 2.1 m telescope in San Pedro Mártir, operated by the Observatorio Astronómico Nacional (OAN/SPM) in Baja California, México. Images were obtained under photometric conditions on 1997 January 24 through the broad-band filter K' (2.125 μm, Δλ = 0.35 μm)¹, and narrow-band filter cK (2.26 μm, Δλ = 0.06); and on January 27 through the broad-band filters J (1.20 μm, Δλ = 0.28 μm) and H (1.60 μm, Δλ = 0.27 μm), and narrow-band filter H₂ v=1-0 S(1) (2.122 μm, Δλ = 0.02 μm). Five added object images were processed by subtracting a median-filtered image of four nearby sky frames taken with the same exposure times at adjacent po-

¹ This is the Barr Associates filter known as Mauna Kea K'

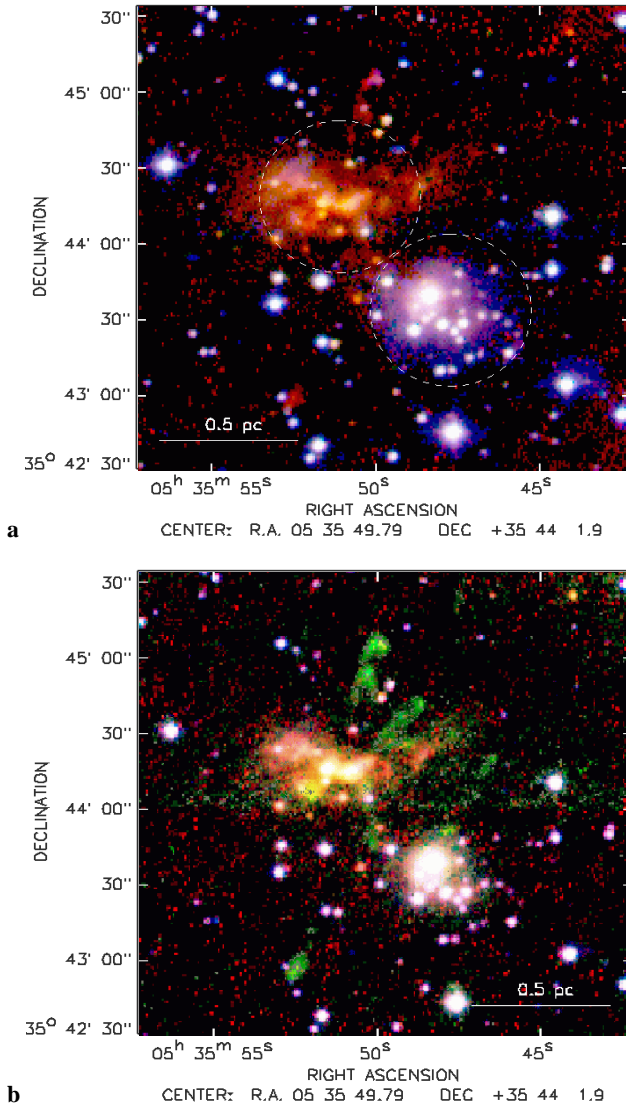


Fig. 2a and b. Composite NIR color images of the region around IRAS05358+3543. **a** Shows emission in J (blue), H (green) and K' (red). This field covers $3.1' \times 3.1'$ which corresponds to $1.6 \text{ pc} \times 1.6 \text{ pc}$ at $D=1.8 \text{ kpc}$. Two groups of stars (NE and SW clusters) are revealed, as well as several nebular features spread from North to South across the image, shown in red. Dashed circles of $1'$ in diameter are drawn around each cluster to clarify the location of the NE and SW clusters. **b** Shows emission in H (blue), H₂ (green) and cK (red). Note that H₂ nebulosities stand out in green.

sitions to the object. The total integration times were 600 s, 600 s, 900 s, 900 s, and 600 s in J, H, K, H₂ and cK, respectively. The FWHM PSF of the images were $2.3''$ (J), $2.2''$ (H), $2.3''$ (K'), $2.2''$ (H₂) and $2.0''$ (cK). The plate scale of CAMILA was $0.84''/\text{pix}$. The images were flattened by low and high illumination sky flats obtained at sunset. The flux calibration was obtained by observing the UKIRT faint standard stars 18, 19 and 20. The position of the sources in the field is solved linearly from nine optically visible stars in the Digitized Sky Survey, and the resultant positional uncertainty is $1''$. The continuum subtracted image of H₂ was obtained by estimating the continuum from a

weighted average of the continuum K-filter and the H-filter, in order to have a better subtraction for blue objects.

A composite color image (JHK) of the region (see Fig. 2a) shows the presence of two distinct stellar groups where stellar density is enhanced, here on called NE (redder) and SW clusters, based on their location in the S233IR region. Note that the observed field, $3.67' \times 3.67'$, corresponds to $1.92 \times 1.92 \text{ pc}^2$ at $D=1.8 \text{ kpc}$, and so, the projected separation between clusters ($\sim 1'$) is $\sim 0.5 \text{ pc}$. Also, as have been noted by Hodapp (1994), there are some nebular features (see Fig. 2b), probably produced by shock-excited gas discussed in Sect. 4.

2.2. Infrared Fabry-Perot

The observations were carried out at the f/4.5 Cassegrain focus of the same telescope at OAN/SPM. Images under photometric conditions were taken on 1998 October 3. The plate scale was the same as in broad band images and the seeing was $2.2''$ (FWHM). A set of images was obtained at 26 etalon positions (channels) that scan a single order at 9.82 km s^{-1} per channel for H₂ $v=1-0$ S(1) ($2.122 \mu\text{m}$) narrow filter. A complete instrumental setup description of the IR Fabry-Perot interferometer is presented in Salas et al. (1999).

The observing sequence consisted of alternative imaging of the region and a blank sky region $81''$ to the east for each etalon position. The telescope allowed that the on-source image was accurately positioned back within $1''$, eliminating re-centering problems. On-source and sky integration times were 60 s. The typical 1σ noise in any image is $0.07 \text{ counts s}^{-1} \text{ pixel}^{-1}$, while the intensity in extended emission regions of interest goes up $1.0 \text{ count/s/pixel}$. The $2.1332885 \mu\text{m}$ line of the Ar lamp was observed at each etalon position for calibration after the source and sky images, obtaining a velocity uncertainty of 0.5 km/s in the wavelength fit. A series of high and low illumination sky flats at each etalon position were obtained at sunset for flat-fielding.

3. Photometry and results

3.1. Stellar photometry routines

The photometry of the infrared sources in S233IR was obtained with DAOPHOT routines (Landsman 1996) in IDL. DAOPHOT routines for stellar fields were adapted to our infrared images and allowed us to follow a consistent set of reduction routines, useful for any rich stellar field observed with CAMILA. A detailed description of the reduction procedure for IR clusters will be presented by Porras (2000). Point sources were identified with FIND routine, with the detection threshold set to 3σ above the local background. Due to the number of stars in the region we obtained photometry using the PSF fitting algorithm GETPSF. The PSF fitting radius was 3 pixels and the local sky annulus was set from 6 to 8 pixels. Magnitudes were transformed from the UKIRT to the homogenized Glass-Johnson system, using the transformation equations of Bessell & Brett (1988). The intrinsic error in the photometry is less than 7%. We used mean atmospheric extinction coefficients derived by Carrasco et al. (1991) for the observing site.

For the whole region, the differential completeness limits in magnitude are 19, 18 and 17 mag in the J, H and K' filters, respectively. They were obtained as the magnitude at which 99% of stars artificially added with ADDSTAR routine are recovered within a magnitude bin (see Carpenter et al. 1997; Hodapp 1994).

In regions with strong nebulosity the differential completeness limits are 19, 16 and 15 in the J, H and K' filters, respectively. Thus in H and K' the gas component affects the completeness limit by ~ 2 mag. By degrading spatial resolution, we checked that stellar colors are not affected significantly ($< 1\%$) by local background in regions with nebulosity.

By examining the density of stars in the field, we have chosen a $1'$ diameter for the SW cluster, which contains all blue stars without an optical counterpart around a density maxima. For a fair comparison of stellar populations, we have chosen a similar diameter for the NE cluster. Also, we have defined a control region (distributed population) as the region outside these two circles (see Fig. 2a). The distributed population stars, i.e. non cluster, are in excess of expected field galactic contamination, and are called field for short.

JHK luminosity histograms are presented in Fig. 3 for each cluster and field stars. The K-band histogram is quite similar to that obtained by Hodapp (1994) for S233.

Table 1 includes photometric near-infrared data for 98 stars in S233IR. The table is only available in electronic form at the CDS via anonymous ftp to cdsarc.u-strasbg.fr (130.79.128.5) or via <http://cdsweb.u-strasbg.fr/Abstract.html>. Note that 92 stars are detected in JHK and that sources IR 93 to IR 98 are quite red and undetected in J. Five of these red stars are likely members of the NE cluster, since they lie inside the $1'$ circle; while IR 98 lies outside the clusters. If so, the population clearly associated to clusters is of 20 and 15 stars in the SW and NE clusters, respectively. Coordinates (Columns (2) and (3)) were obtained using Skyview optical images using positions common to infrared sources to derive target positions in the usual way. JHK' photometry are presented in Cols. (4), (5) and (6), respectively. The extinction A_V and mass associated to each source is given in Column (7) and Column (8), respectively. The estimation procedure is described in Sect. 3.3 and Sect. 5.4 below.

3.2. Color-color diagram

The J-H/H-K diagram presented in Fig. 4 includes all the detected stars and shows a high population of YSOs. Main sequence stars (here after MS), affected by normal interstellar reddening, are located in the region between the two upper dotted lines in this diagram. Note that this region includes also WTTS and some CTTS, while the region above the CTTS locus is occupied by reddened/near-IR excess CTTS (cf. Meyer 1996). Clear color differences between the two clusters are revealed (cf. Fig. 2a), with NE cluster members as well as nebular gas being much redder.

Unusual colors are observed for IR 39 and IR 57. Source IR 39 ($J-H = 2.08$, $H-K = 0.28$) corresponds to an unresolved pair of stars located in the SW cluster, for which individual photometry

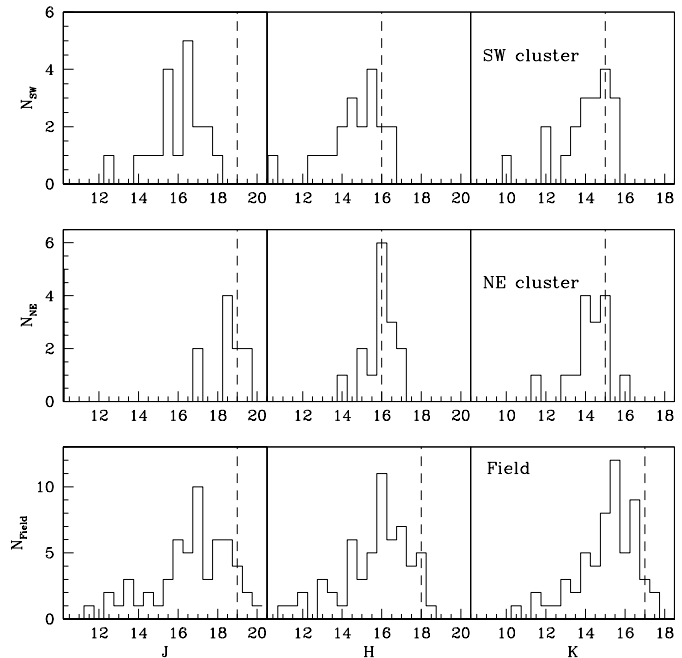


Fig. 3. Luminosity histograms at J, H and K for NE cluster, SW cluster and field stars (non-cluster). Completeness limits are represented by vertical broken lines.

is needed. IR 57 ($J-H = 1.48$, $H-K = 0.18$) is a very bright star located in the western edge of the observed field, surprisingly it does not have an optical counterpart and seems not to be related with any of the clusters. IR 23 is a deeply embedded MS star ($J-H = 2.53$, $H-K = 0.99$) not located in any of the clusters.

In each cluster we have counted the population of stars with near-IR excesses, i.e. those located to the right of the MS reddening line: 40% (6/15) for the NE cluster, 30% (6/20) for the SW cluster and 29% (15/51) for field stars. It should be noted that 5 sources in the NE cluster are not detected in the J-band so their J-H color is unknown while in H-K are extremely red. This may increase the percentage of IR-excess stars in the NE cluster up to 80%. Also, we have only considered stars in the J-H/H-K diagram located above 1σ from the CTTS locus. We consider foreground stars (6) based on $A_V < 1.8$, $J-H < 1$ and $H-K < 0.4$, which are omitted from our analysis.

Leaving flexible the parameter of roundness, IDL / DAOPHOT procedures can also find and calculate the photometry of objects that are not stellar. Such is the case of a pair of H₂ nebulosities N1 and N2 (see Sect. 4 below), for which photometric data was available. Their positions in the J-H/H-K diagram are quite distinct from stellar sources, but are in agreement with the theoretical region predicted by Smith (1995) for molecular shocks.

3.3. Extinction

The computation of the extinction to individual stars depends on its location in the J-H/H-K diagram. Those in the locus of reddened MS stars are de-reddened using the corresponding J/J-H diagram for an adopted distance of 1.8 kpc presented in Fig. 5.

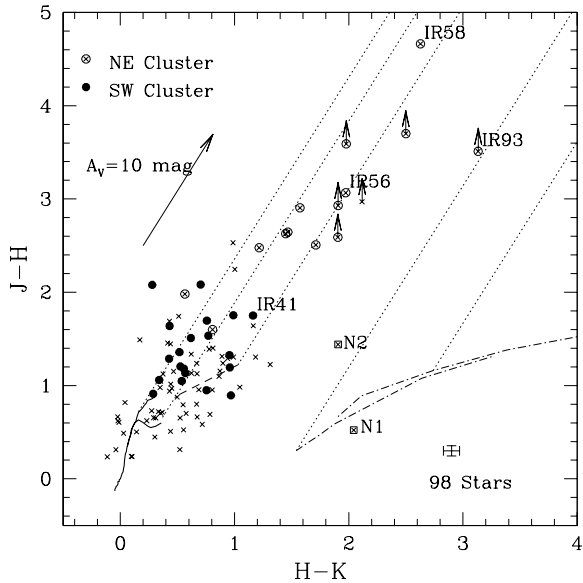


Fig. 4. Color-color diagram of the stars around IRAS 05358+3543. The main sequence and red giant branch are drawn with solid lines (Bessell & Brett 1988). The dashed line shows the CTTS locus (Meyer 1996). The dotted lines follow the direction of the interstellar reddening vector A_V . We used different symbols for stars inside a circle of $1'$ in diameter centered in each of the two clusters, (\bullet) for SW cluster members and (\otimes) for NE cluster members, while field stars are shown as \times . Arrows indicate lower limits for stars without J counterpart. In the lower right part of the diagram, N1 and N2 show the location of the brightest H₂ knots (see Sect. 4.1) detected and the dash-dotted lines correspond to J- and C-shock models from Smith (1995). Sources IR 41, IR 56, IR 58 and IR 93 are labeled to indicate the position of four candidate stars possibly responsible of HH activity in the region (see Sect. 5.1). In the lower right corner the average photometric error cross is indicated.

While those at positions of reddened CTT and/or Ae/Be stars are de-reddened directly in the J-H/H-K diagram, based on their distance to the CTTS line (Meyer 1996). Each cluster has both MS and CTT stars. Individual A_V values are listed in Table 1.

The estimated average extinction of the SW cluster is $A_V = 8.44 \pm 4.77$ mag for 18 stars, which excludes the unresolved pair IR 39 with $A_V = 17.9$ and IR 35 which lies $>1\sigma$ below the CTTS line. While, for the NE cluster $A_V = 15.06 \pm 3.48$ mag for 9 stars, excluding IR 58 because this extremely red star has an anomalous extinction, at least twice the average value. IR 58 must be a deeply embedded YSO ($A_V \sim 30.14$ mag) with intrinsic reddening likely produced by a protostellar disk. The mean A_V is assumed for stars IR 93 to IR 97, possible members of the NE cluster. For 40 field stars, i.e. distributed population stars and associated to S2331R, we obtain $A_V = 4.88 \pm 4.48$. Due to the uncertainty in distance to S2331R we calculate that the effect on A_V for twice the distance is that the mean value increases by $\sim 8\%$.

4. Molecular hydrogen

The molecular hydrogen emission in S2331R is presented in the composite color image in Fig. 2b. H₂ nebulosities are shown

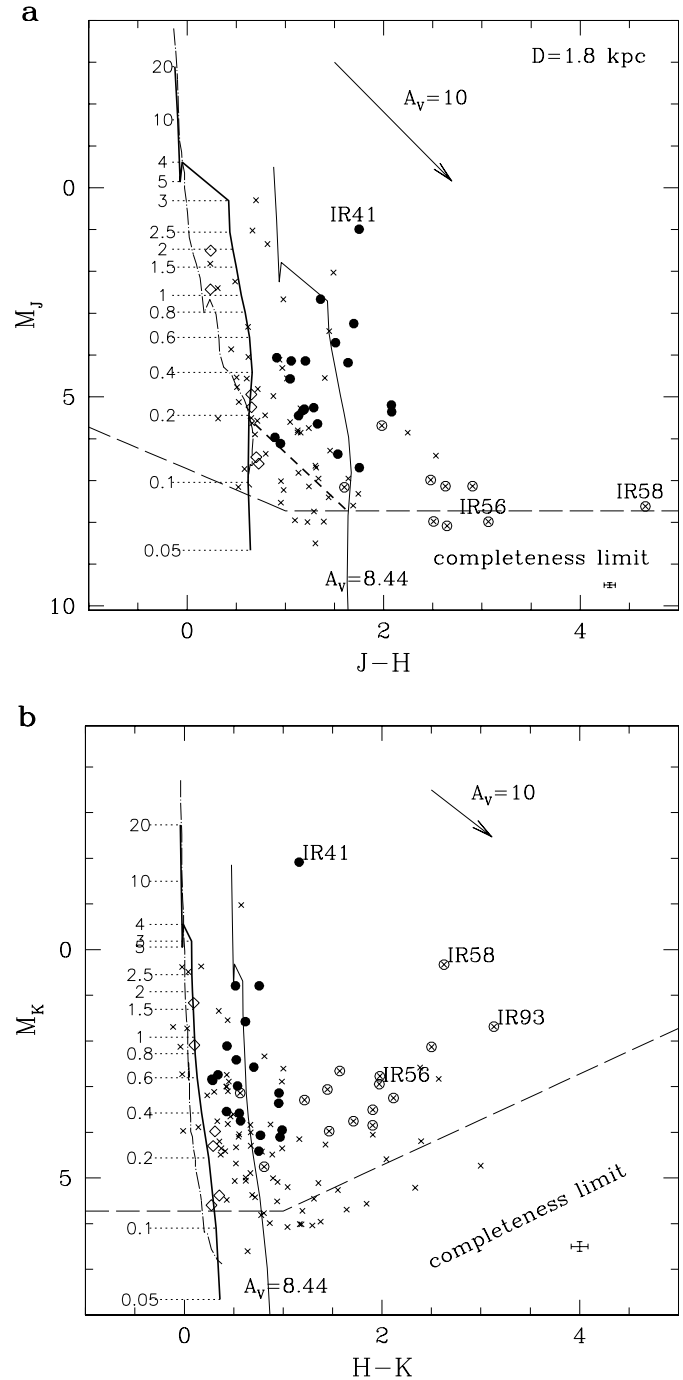


Fig. 5a and b. Color-magnitude diagrams at the adopted $D = 1.8$ kpc (distance modulus 11.28). **a** J vs. J-H and **b** K vs. H-K. Symbols are the same as in Fig. 4, except that (\circ) correspond to foreground stars (see Sect. 3.2). Sources IR 41, IR 56, IR 58 and IR 93 are labeled. Completeness limits in magnitude are represented as a long-dashed line. The main sequence is drawn with a dash-dotted line. The solid almost vertical curve represents the 3 Myr (estimated age of SW cluster) isochrone with stellar masses given along it (cf. Sect. 5.3). It is also shown at the mean extinction of the SW cluster ($A_V = 8.44$). The diagonal short-dashed line marks the region of stars with $M > 0.2 M_{\odot}$, the mass completeness limit. Extinction vector and average error cross (lower right) are also indicated.

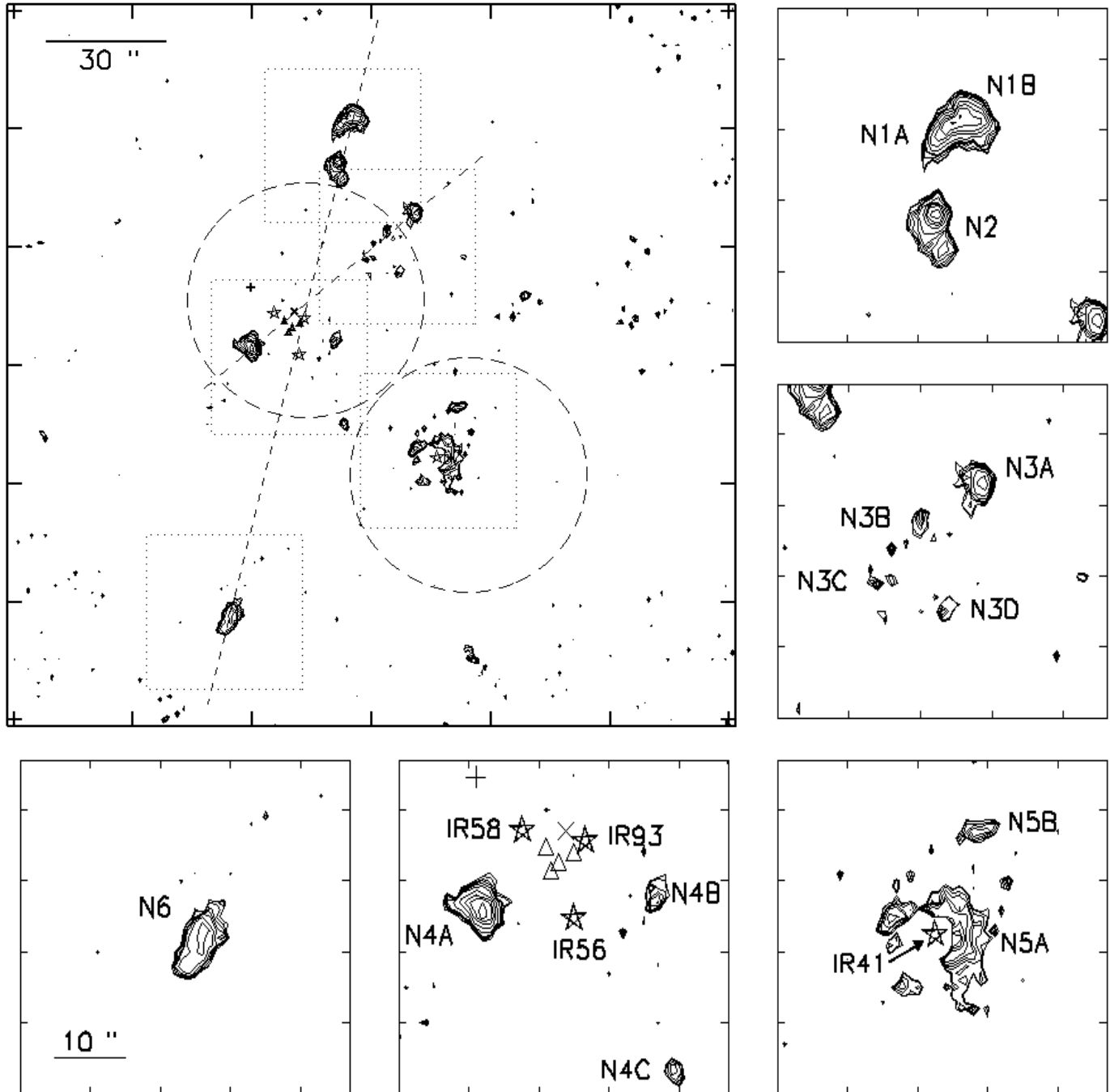


Fig. 6. Contour maps of molecular hydrogen emission. The knots are labeled N1 to N6. Some nebulosities have multiple components labeled A, B, C and D. The scale is presented on the lower left insert. Possible exciting stars (\star) and masers of water (\triangle), hydroxyl ($+$) and methanol (\times) are shown.

in green and clearly stand out from the extended nebulosities shown in Fig. 2a.

4.1. Morphology of H₂ nebulosities

Emission of the molecular hydrogen is mainly associated to six nebular structures shown in Fig. 6, where the continuum subtracted H₂ emission is presented. By comparison with the image in Fig. 2a most of the extended emission at K' is produced by

molecular hydrogen. We have designated the H₂ knots or nebulosities as N1 to N6, where the N stands for “nudo” or nebulosity. Detailed contour maps of each H₂ nebulosity show that some consist of several components as is shown in the inserts in Fig. 6. The position, fluxes and sizes of H₂ nebulosities are presented in Table 2.

N1 is the only feature with a clear bow shock morphology pointing North and has two intensity peaks A and B. N1 is also the brighter source detected in H₂. N2 lies very close to

Table 2. Properties of Molecular Hydrogen Nebulosities in the S233IR Region

Source (1)	α_{1950} (2)	δ_{1950} (3)	I_{max}^1 (4)	$Flux^2$ (5)	Size ³ (6)	I_{peak}^V ⁴ (7)	V_{peak} ⁵ (8)
N1A	05 35 50.07	+35 45 05.66	1.04	7.92	6.7 × 5.0	0.75	-25.2
N1B	05 35 50.07	+35 45 05.66	1.04	7.92	6.7 × 5.0	0.73	-21.2
N2	05 35 50.41	+35 44 54.02	0.82	4.57	4.2 × 6.7	0.66	-14.4
N3A	05 35 48.81	+35 44 41.38	0.54	2.82	5.0 × 4.2	0.32	-22.2
N3B	05 35 49.35	+35 44 35.65	0.40	1.02	4.2 × 2.5		
N3C	05 35 49.70	+35 44 29.00	0.38	0.91	4.2 × 2.5		
N3D	05 35 49.23	+35 44 26.53	0.42	0.64	3.4 × 1.7		
N4A	05 35 51.69	+35 44 15.59	1.00	5.59	5.0 × 4.2	0.7	-7.5
N4B	05 35 50.49	+35 44 08.55	0.43	0.72	2.5 × 2.5		
N4C	05 35 50.25	+35 43 47.99	0.37	1.01	3.4 × 3.4		
N5A	05 35 52.58	+35 42 58.87	0.53	12.07	12.6 × 15.1		
N5B	05 35 47.89	+35 43 51.59	0.49	1.08	3.4 × 2.5		
N6	05 35 52.64	+35 42 58.35	0.73	3.83	4.2 × 5.0	0.38	-17.3

¹ Peak intensity in units of 10^{-4} erg s⁻¹ cm⁻² sr⁻¹ ² Total flux in units of 10^{-14} erg s⁻¹ cm⁻² ³ Size in arcsec ⁴ Peak intensity of Lorentzian fit in units of count/s/channel/pixel ⁵ Peak velocity of Lorentzian fit (LSR) in km/s

N1, located to the South. N2 is more elongated and has also two maxima. Both, N1 (IR 81) and N2 (IR 77) are the only nebulosities for which J, H and K' photometry could be obtained (cf. Table 1). Their colors are in agreement with the theoretical region for molecular J- and C-shock predicted by Smith (1995).

N3 is a chain of small knots linked by weak traces of H₂ gas. Three of them, N3A, N3B and N3C, appear aligned towards IR93 and with the same alignment pattern that H₂O masers trace (Tofani et al. 1995). N4 is a group of three knots around the center of the NE cluster and the stars IR 56, IR 58 and IR 93. N4A is the brightest and extended of the group and also aligned with the chain N3 + IR93 + H₂O maser. H₂O and CH₃OH masers are located in the region between N4A and N4B. This configuration suggests that N3A and N4A are a jet/counter-jet system produced by source IR93.

N5A shows extended and almost spherical emission around the source IR41 which lies closer to the IRAS source position. Several stars in the N5A field did not allow the full detection of this extended nebulosity. It resembles a reflection nebulosity possibly produced by fluorescence (Black & van Dishoeck 1987) instead of shocks. N5B is separated from N5A and located to the NW, possibly aligned with a very weak group of H₂ features. Finally, N6 is an elongated and isolated knot located towards the SE of S233IR, maybe the counter-jet of N1 and N2.

The positions of knots N1, N2 and N6 describe a line that crosses IR 56 and IR 93, which are the exciting source candidates of these H₂ nebulosities. The morphology and fluxes (Table 2) indicate that they might be part of Herbig-Haro objects in a region of very high extinction, only detectable in the infrared. Radio continuum sources should confirm the nature and location of the exciting source(s). Similar H₂ nebulosities associated to HH objects have been previously discussed (e.g. Lane 1989; Miralles et al. 1997; Zinnecker et al. 1997; Salas et al. 1998; Salas et al. 1999). The association of N4A+N3A and N1+N6 is suggested by the coincidence in exciting source (IR93). We

note that most of the H₂ knots are associated with the youngest and reddest cluster, where the GMC core is also located.

4.2. H₂ velocity field

The scanning Fabry-Perot images show emission mainly in 5 channels with velocities -36.9 to 2.3 km/s (all velocities referred to LSR). All the nebulosities show a maximum intensity at velocity channel -17.3 km/s, which is consistent with the GMC rest velocity by Cesaroni et al. (1999) (-15.6 km/s, FWHM~3.4 km/s), as well as the other molecular tracers.

The detailed kinematics of H₂ gas is presented in Fig. 7, that shows the individual spectra at the position of the knots, averaged in 3×3 pixel boxes. The FWHM in the H₂ lines is typically 3 channels (30 km/s), which is wider than the instrumental response (2.4 channels or 23.6 km/s). The observed profiles were fit by Lorentzians which are shown as continuous curves in Fig. 7. The peak velocity and intensity parameters for several knots are presented in Columns (7) and (8) of Table 2. Intensities are given in count/s/channel/pixel and have typical errors of 0.05 in these units, while velocities are given in km/s (LSR) with typical uncertainties of 5 km/s. The velocity of the GMC associated to the H II region S233 reported by Cesaroni et al (1999) is indicated in Fig. 7 as a vertical dotted line. As can be seen from the spectra of 6 H₂ nebulosities: 2 show velocities close to the CO velocity (N2 and N6), 3 are blue-shifted (N1E, N1W and N3A) and N4A is red-shifted.

As is shown in Table 2 (cf. Fig. 2b), knot N1 has a bow shock structure and the two components show similar peak velocities (N1A = -25.2 km/s and N1B = -21.2 km/s), while knots N2 and N6 are slightly redder (-14.4 and -17.3 km/s, respectively) with a velocity consistent with the ambient quiescent medium. The observed velocities reinforce their relation and suggest that they lie on the plane of the sky. The orientation and location of knots N3A (-22.2 km/s) and N4A (-7.5 km/s) suggest that they may

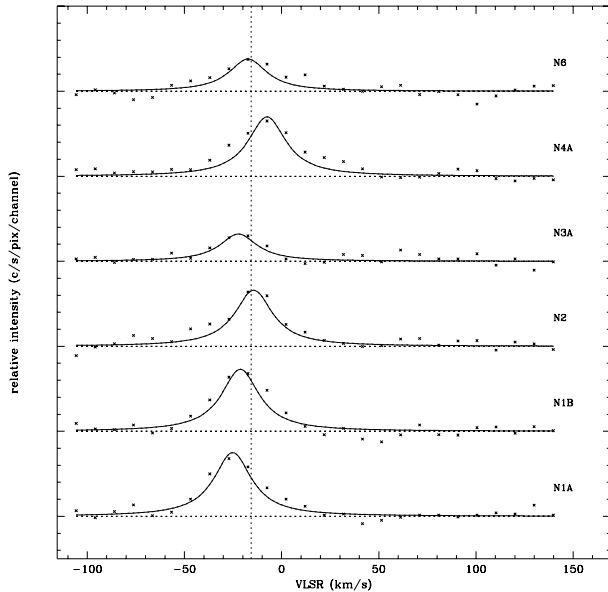


Fig. 7. Velocity components of H₂ knots in the region S233IR, the crosses are the observed relative intensities in units of counts/s/pixel/channel and the continuous line is the Lorentzian fit. The vertical dotted line indicates the ambient CO velocity.

form a jet/counter-jet structure oriented to the observers view angle, with knot N4A being the reddest.

The molecular hydrogen nebulosities show velocities consistent with the maser emission peak velocities located near knot N4A (-7.5 km/s): H₂O (-16.9, -17.5, -15.6 and -12.9 km/s; Tofani et al. 1995), CH₃OH (-17 to -10 km/s; Menten 1991) and OH (-11 km/s; Wouterloot et al. 1988). The association between the masers and H₂ nebulosities is reinforced by the similarity in their velocities and are possibly all tracing an outflow/jet emanating from source IR 93 towards knots N4A and N3A.

5. Discussion

5.1. Two young stellar clusters (YSCs) and molecular outflow

Evidence for the presence of two distinct YSCs in the S233IR region based on the NIR study are: stellar colors, extinction to NE cluster is ~ 7 magnitudes larger than that to the SW cluster, higher population of NIR excess stars in NE cluster, presence of shocked H₂ emission driven by a young star probably associated to the NE cluster. Also, 3 different types of masers are detected in the area of the NE cluster and none associated to the SW cluster. Cesaroni et al. (1999) show that observed molecules trace a core in the H₂O masers positions. Felli et al. (1992) suggest a common energy source for the H₂O maser emission and CO molecular outflows, most probably the stellar wind of a YSO. H₂O and OH maser positions are in agreement with the evolutionary sequence suggested by Forster & Caswell 1989, who suggest that H₂O masers form near the core of a massive protostar while OH masers form in the less dense circumstellar material before the accretion onto the YSO terminates ($\sim 10^5$ years). Menten (1991) identifies the methanol maser (CH₃OH)

observed in this region as Class I; and Plambeck & Menten (1990) argue that Class I masers may be formed where molecular outflows shock preexisting dense clumps in a massive star forming region (see Fig. 6). The kinematic association of H₂O masers, the H₂ clumps and the GMC core discussed in Sect. 4.2, are all evidence of a molecular outflow emanating from a YSO (possibly IR 93) located in the NE cluster of young stars.

Based on relative positions between stars and H₂ nebulosities, we select four possible candidates as exciting sources of the CO outflow: IR 56, IR 58, IR 93 and IR 41. The HH system composed by knots N1, N2 and N6 has three possible exciting sources; two embedded CTTS IR 56 ($A_V = 15.49$ mag) and IR 58 ($A_V > 30$ mag), and IR 93 which has no counterpart in the J-filter, is the reddest source in the observed field and has a nebular feature directed in the direction of knots N3 (cf. Fig. 2). These stars have a steep SED in the NIR. Both IR 56 and IR 93 lie in the path of the line across knots N1, N2 and N6, while IR 58 lies 7'' to the east. However, the location of masers and GMC core, as well as the kinematical association of the core, masers and H₂ nebulosities, indicate that most probably IR 93 is the exciting source of the molecular outflow. This source is also responsible of the two jet/counter-jet H-H like systems: N1+N6 and N4A+N3A, detected as shocked H₂. A radio continuum study of this region should confirm the location of the exciting source for the molecular outflow, with no clear bipolar structure (Snell et al. 1990), and H₂ shocked gas.

IR 41 is located far from the masers and in the SW cluster, most likely associated to IRAS 05358+3543 rather than the outflow. Its location in the J/J-H and J-H/H-K diagrams suggests an intrinsically luminous source with IR-excess, i.e. a class II Herbig Ae/Be candidate, according to the classification by Hillenbrand et al. (1992). It is responsible for the H₂ emission around it (N5A), possibly produced by fluorescence instead of shocks.

5.2. Age estimation

It is not easy to estimate the age of a young stellar cluster without spectroscopic data combined with photometric results. Nevertheless, we can attempt a crude age estimate for a SFR based on a comparison between observed and theoretical luminosity function histograms. The models presented by Zinnecker et al. (1993) and Strom et al. (1993) for K-band and J-band absolute luminosity functions, respectively, provide the necessary KLF and JLF model histograms. Both models are based on the assumption of coeval star formation, use the pre-main sequence isochrones by D'Antona & Mazzitelli (1994) and consider the IMF of Miller & Scalo (1979). The use of JLF is preferred since J provides a more reliable estimate of the true photospheric emission.

Strom et al. (1993) trace six different evolutionary histograms at ages of 0.3, 0.7, 1, 3, 7 and 10 Myr which can be used to construct a matrix \widehat{M} where each column contains the theoretical JLF at each age. Then $\overline{JLF} = \widehat{M} \vec{E}$, where \overline{JLF} is the J-luminosity function and \vec{E} is defined as an age vector, usually considered a Delta function. On the other hand, \widehat{M} is an

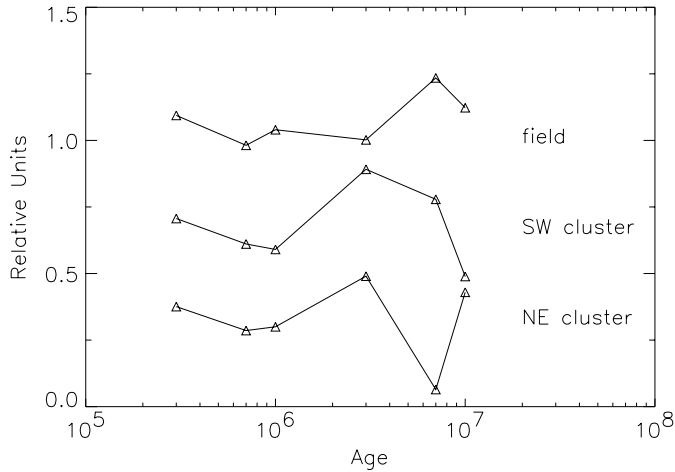


Fig. 8. Age vectors representing the distribution of stars in all ages for S233IR. Offsets in ordinate of 0.31, 0.65 and 0.99 have been applied to data of NE, SW and field, respectively. Estimated age is obtained from maximum value via a parabola fit.

influence matrix and can be used to estimate an age vector \vec{E} , from the observed JLF (\vec{JLF}_{obs}) for each cluster, by means of the transformation:

$$\vec{E} = (\widehat{M}^T \widehat{M})^{-1} \widehat{M} \vec{JLF}_{obs}$$

The elements in \vec{E} give the distribution of stars in all ages and the age estimate can be obtained with the maximum value. We note that the distributions have to be normalized to the number of stars in the region.

This method is applied to S233IR where we derived \vec{E} for each cluster and field stars. The results are presented in Fig. 8. We fit a parabola to the maximum peak and adjacent points to estimate the following ages: $\lesssim 2$ Myr for NE cluster, 3 Myr for SW cluster, 6 Myr for field (distributed population) stars.

Alternatively, we can apply a K-S test to the observed and theoretical histograms (JLF) to estimate ages: 0.7 Myr for NE cluster, 1 Myr for SW cluster, 7 Myr for field stars. Finally, the estimates by-eye from the best match of theoretical and observed JLF: 1 Myr for NE cluster, 3 Myr for SW cluster, 7 Myr for field stars. Although, the NE cluster has a small number of sources and age estimates are less reliable, the presence of several tracers of star formation, including more deeply embedded reddened sources, reinforce that this cluster is younger than the SW cluster. The three methods are consistent and show that $\text{age(NE)} < \text{age(SW)} < \text{age(field)}$ with the three dominated by a population of PMS objects and smaller than the expected lifetime of a GMC.

Model histograms of JLF at available ages and observed ones are presented in Fig. 9. For SW cluster and field stars we find a reasonable match and a turnover well above the completeness limit. This is not the case for the NE cluster, where only the bright tail of the distribution is detected and a turnover is missing.

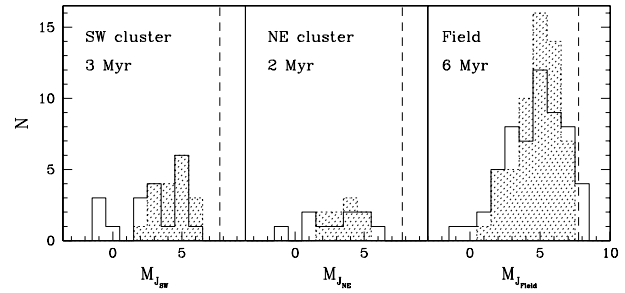


Fig. 9. Observed JLF histograms and the corresponding age for SW cluster, NE cluster and field stars. Shaded histogram corresponds to the theoretical model by Strom et al. (1993) at 3 Myr (SW), 1 Myr (NE) and 7 Myr (field). Completeness limits are represented by vertical broken lines.

5.3. Isochrones in the J/J-H diagram

The construction of isochrones in the J/J-H diagram is obtained from pre-main sequence evolutionary tracks by D'Antona & Mazzitelli (1994), assuming Alexander opacities and the Canuto & Mazzitelli convection model, at ages 0.1, 0.3, 1, 3, 10, 30 and 100 Myr. For $M > 2.5 M_{\odot}$ we used the tracks presented by Hillenbrand et al. (1995). For each stellar mass M the corresponding luminosity L and effective temperature T_e are obtained. From L we derive $M_{bol} = 4.74 - 2.5 \log(L/L_{\odot})$ (Bessell et al. 1998) and from T_e the bolometric correction is obtained from Flower (1996), which allows to calculate $M_V = M_{bol} - BC$. Also from T_e , the colors V-J and J-H for dwarfs are obtained from Bessell & Brett (1988), using the T_e values of Tokunaga (2000). Finally, magnitude $J = M_V - (V - J)$.

In Fig. 5 the isochrone shown corresponds to the estimated age of the SW cluster, along this line the corresponding stellar mass values are clearly indicated. If this isochrone is moved along the extinction vector to the mean value $A_V = 8.44$, we can check the completeness in mass that we are able to detect based on the magnitude limits imposed by our observations ($J = 19$, $H = 18$). It is clear that stars in the SW cluster of masses from 0.2 to 10 M_{\odot} are detected and only the very low-mass end of dwarf stars is missed. This is also the case for field stars ($A_V = 4.88$). The IMF construction of the SW cluster and field stars, presented below, is then justified. This is not the case for the NE cluster, which is deeply embedded ($A_V = 15.06$) and is complete only for $M > 1 M_{\odot}$.

5.4. IMF

We derive masses by a two step procedure. First, we identify in the J-H/H-K diagram reddened MS and CTT and/or Ae/Be stars. The mass of MS reddened stars can be obtained from the J/J-H diagram by de-reddening them to the appropriate isochrone. For stars in the SW cluster we used the 3 Myr isochrone, while for field stars we used the 7 Myr one. In the case of reddened CTT and Ae/Be stars, we use the empirical relations from Carpenter et al. (1993): $\log M = -0.25 M_H + 0.44$ and $\log M = -0.24 M_K + 0.24$, where M_H and M_K are the uncorrected for extinction H- and K-band magnitudes, as assumed

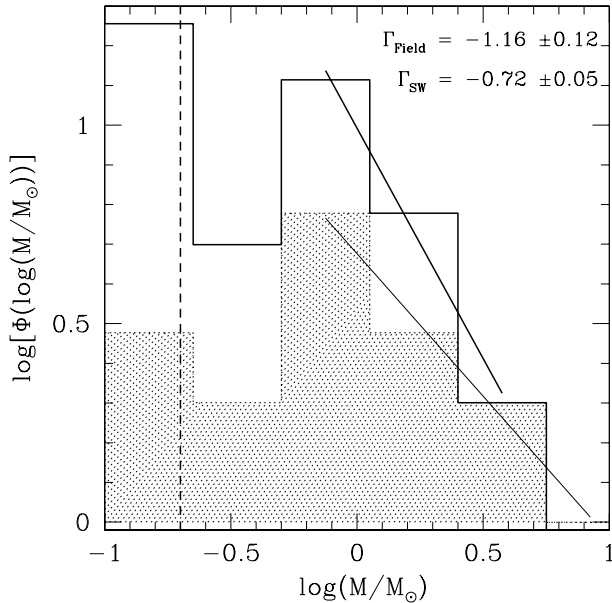


Fig. 10. IMF histogram of the SW cluster (shaded) and field stars (empty) in the S233IR region using bins of 0.35 in $\log M$. Note that the y-axis is $\log\Phi(\log M)$. Slope values (Γ) obtained for $\log M > -0.5 M_{\odot}$ are given on top. The broken vertical line represents the completeness limit in mass for the SW cluster, for field stars this limit is slightly to the left.

by Carpenter et al. (1993). We note that if an A_V of 10 mag is required, this would imply an underestimation of the mass of 0.24 dex.

With this method we obtained the spectrum of masses for the SW cluster and field stars shown in Fig. 10. In the IMF we only include non biased stars, i.e. those with $A_V < 8.4$ and $M > 0.2 M_{\odot}$, where the sample is considered complete. The completeness limit in mass estimated for the SW cluster ($0.2 M_{\odot}$), suggests that the turnover in the IMF for $M < 1 M_{\odot}$ is probably real. A least squares fit from the peak value to high-mass stars considering stars with $\log M > -0.5 M_{\odot}$ and bins of 0.35 in $\log M$ is applied. The slope value ($\Gamma = d \log\Phi(\log M)/d \log M$) of SW cluster stars is $\Gamma_{SW} = -0.72 \pm 0.05$ flatter than Salpeter's value; while for field stars $\Gamma_{field} = -1.16 \pm 0.12$, consistent with Salpeter value of -1.35 (Salpeter 1955). However, spectroscopic follow-up in S233IR is required to estimate stellar temperatures and a reliable estimation of the stellar IMF.

As suggested by Meyer et al. (2000) the best diagnostics in YSCs is the ratio R of intermediate-to-low-mass stars (cf. their Fig. 3 and Table 1). We consider for S233IR the completeness limit in mass achieved here and compute: $R = N(1 - 10M_{\odot})/N(0.2 - 1M_{\odot})$. We obtain $R_{field} = 8/36 = 0.22 \pm 0.09$, which is more consistent with a Salpeter IMF, according to Meyer and co-workers, and in agreement with its slope value Γ_{field} , and $R_{SW} = 6/13 = 0.46 \pm 0.23$, according to Meyer and co-workers, consistent with a Miller & Scalo (1979) IMF thus implying a turnover in the IMF for low-mass stars that is seen in Fig. 10. For the NE cluster we detected 3 intermediate-mass

stars ($M > 1 M_{\odot}$) down to our completeness limit. Seven deeply embedded low-mass stars are detected thanks to their large IR excesses, but completeness cannot be attained by any means. We can only assert that $R_{NE} < 0.4 \pm 0.30$, a value compatible with both Miller & Scalo and/or Salpeter IMF (see Meyer et al. 2000).

6. Conclusions

1. Direct J, H and K' images and photometric results of the S233IR region reveal the existence of two young embedded clusters near IRAS 05358+3543, separated by ~ 0.5 pc at $D = 1.8$ kpc. The average extinction values A_V obtained are: 8.44 ± 4.77 mag (SW cluster), 15.06 ± 3.48 mag (NE cluster) and 4.88 ± 4.48 mag (field or distributed population).

2. Emission from molecular hydrogen is mainly associated to six nebular structures, most likely produced by shocks with similar properties as deeply embedded Herbig-Haro objects. Most of them are directly associated to the NE cluster, where several tracers of star formation activity have been detected.

3. The H₂ emission velocity field and peak velocities are consistent with the GMC rest velocity and H₂O maser peak velocities. Morphology and velocities show that two jet/counter-jet structures produced by shocks are present in the field. Nebulosity N6 is the redder part of a bipolar jet emanating from the center of the NE cluster, while N1 (bow-shock structure) and N2 are the bluer counterpart. Nebulosities N4A and N3A trace a second jet/counter-jet system.

4. A group of candidate stars responsible for the H₂ emission is considered. Source IR 41 related with IRAS 05358+3543 and associated to the bluer cluster (SW), seems to be the exciting source of fluorescence H₂ emission around it. Most probably IR 93, located near the center of the NE cluster, produces the molecular outflow emission and HH activity in the S233IR region. Radio continuum studies are needed to locate the outflow driving source and its association to IR 93.

5. The presence of young stars, molecular outflow, GMC core and masers related with the NE cluster, as well as the presence of HH-like activity and stellar colors, strongly suggest that the NE cluster is younger than the SW cluster.

6. Luminosity function histograms are used to obtain an age vector, that gives the age distribution of stars. The maximum value gives the age estimate: $\lesssim 2$ Myr for NE cluster, 3 Myr for SW cluster and 6 Myr for field (distributed population) stars. This age trend is confirmed with age estimates based on K-S test and fits by-eye of observed histograms to model JLF. This confirms that the NE cluster is younger and suggest at least two star-formation episodes in the region. The distributed population, in excess of expected field galactic contamination, show ages significantly larger than the cluster members and smaller than the expected lifetime of a GMC, still consistent with a PMS population.

7. IMF slope of SW cluster members $\Gamma_{SW} = -0.72 \pm 0.05$, is consistent with a Miller & Scalo IMF, and $\Gamma_{field} = -1.16 \pm 0.12$ for the distributed population is close to Salpeter's value. The ratio of intermediate to low-mass stars obtained are:

$R_{SW} = 0.46 \pm 0.23$, consistent with a Miller & Scalo IMF, thus implying a turnover for low-mass stars which is observed; while $R_{Field} = 0.22 \pm 0.09$ is consistent with a Salpeter IMF; and we can only assert that $R_{NE} < 0.4 \pm 0.3$ due to completeness limitations. Both R values and IMF slopes indicate similar results in the possible mass spectrum, but follow up spectroscopy is needed.

Acknowledgements. We thank the OAN/SPM technical support group and night assistants, G. García, F. Montalvo and S. Monroy, for their valuable help during the observations. Our special thanks to Leonid Georgiev, our IDL guru, for his help and comments at the early stage of reduction. Our appreciation to the referee Catherine Dougados, for a careful revision of the manuscript, whose comments and suggestions greatly improved the final version. This work has been financed by grant IN-501694 and IN-120198 from DGAPA (UNAM). A. Porras acknowledges a CONACYT (México) scholarship during her graduate studies. Finally, we thank A. Sobolev for his comments.

References

- Bessell M.S., Brett J.M., 1988, *PASP* 100, 1134
 Bessell M.S., Castelli F., Plez B., 1998, *A&A* 333, 231
 Black J.H., van Dishoeck E.F., 1987, *ApJ* 322, 412
 Bronfman L., Nyman L.-A., May J., 1996, *A&AS* 115, 81
 Carpenter J.M., Snell R.L., Schloeb F.P., Skrutskie M.F., 1993, *ApJ* 407, 657
 Carpenter J.M., Meyer M.R., Dougados C., Strom S.E., Hillenbrand L.A., 1997, *AJ* 114, 198
 Carrasco L., Recillas-Cruz E., García-Barreto A., Cruz-González I., Serrano A., 1991, *PASP* 103, 987
 Casoli F., Combes F., Dupraz C., Gerin M., Boulanger F., 1986, *A&A* 169, 281
 Cesaroni R., Felli M., Walmsley C.M., 1999, *A&AS* 136, 333
 Cruz-González I., Carrasco L., Ruiz E., et al., 1994, In: Crawford D.L., Craine E.R. (eds.) *Instrumentation in Astronomy VIII*, Proc. SPIE 2198, p. 774
 Chan G., Fich M., 1995, *AJ* 109, 2611
 Chan S.J., Henning T., Schreyer K., 1996, *A&AS* 115, 285
 D'Antona F., Mazzitelli I., 1994, *ApJS* 90, 467
 Evans N.J. II, Blair G.N., 1981, *ApJ*, 246, 394
 Felli M., Palagi F., Tofani G., 1992, *A&A* 255, 293
 Fich M., Blitz L., 1984, *ApJ* 279, 125
 Flower P.J., 1996, *ApJ* 469, 355
 Forster J.R., Caswell J.L., 1989, *A&A* 213, 339
 Henning T., Cesaroni R., Walmsley M., Pfau W., 1992, *A&AS* 93, 525
 Heyer M.H., Carpenter J.M., Ladd E.F., 1996, *ApJ* 463, 630
 Hillenbrand L.A., Strom S.E., Vrba F.J., Keene J., 1992, *ApJ* 397, 613
 Hillenbrand L.A., Meyer M.R., Strom S.E., Skrutskie M.F., 1995, *AJ* 109, 280
 Hodapp K.-W., 1994, *ApJS* 94, 615
 Hughes V.A., MacLeod G.C., 1989, *AJ* 97, 786
 Israel F.P., Felli M., 1978, *A&A* 63, 325
 Landsman W.B., 1996, *IDL Astronomy User's Library*. In: <http://idlastro.gsfc.nasa.gov/homepage.html>
 Lane A.P., 1989, from *Herbig-Haro Objects and Bipolar Flows*. In: Reipurth B. (ed.) *Proc. ESO Workshop on Low Mass Star Formation and Pre-Main Sequence Objects*. ESO, Garching, p. 331
 Menten K.M., 1991, *ApJ* 380, L75
 Meyer M.R., 1996, Ph.D. Thesis, University of Massachusetts
 Meyer M.R., Adams F.C., Hillenbrand L.A., Carpenter J.M., Larson R.B., 2000, *Clusters and Theoretical Perspectives*. In: Mannings V., Boss A.P., Rusell S.S. (eds.) *Protostars and Planets IV*, in press
 Miller G.E., Scalo J.M., 1979, *ApJS* 41, 513
 Miralles M., Salas L., Cruz-González I., Kurtz S., 1997, *ApJ* 488, 749
 Palagi F., Cesaroni R., Comoretto G., Felli M., Natale V., 1993, *A&A* 101, 153
 Plambeck R.L., Menten K.M., 1990, *ApJ* 364, 555
 Porras A., 2000, Ph.D. Thesis (in preparation)
 Porras A., Cruz-González I., Salas L., 2000, (in preparation)
 Richards P.J., Little L.T., Heaton B.D., Toriseva M., 1987, *MNRAS* 228, 43
 Salas L., Cruz-González I., Porras A., 1998, *ApJ* 500, 853
 Salas L., Rosado M., Cruz-González I., et al., 1999, *ApJ* 511, 822
 Salpeter E.E., 1955, *ApJ* 121, 161
 Schreyer K., Henning T., Koempe C., Harjunpää P., 1996, *A&A* 306, 267
 Smith M.D., 1995, *A&A* 296, 789
 Snell R.L., Dickman R.L., Huang Y.-L., 1990, *ApJ* 352, 139
 Strom K.M., Strom S.E., Merrill M., 1993, *ApJ* 412, 233
 Tofani G., Felli M., Taylor G.B., Hunter T.R., 1995, *A&AS* 112, 299
 Tokunaga A.T., 2000, In: Cox A.N. (ed.) *Allen's Astrophysical Quantities*. Springer-Verlag, New York, p. 143
 Wilking B.A., Blackwell J.H., Mundy L.G., Howe J.E., 1989, *ApJ* 345, 257
 Wood D.O.S., Churchwell E., 1989, *ApJ* 340, 265
 Wouterloot J.G.A., Henkel C., Brand J., 1988, *A&A* 191, 323
 Wouterloot J.G.A., Brand J., 1989, *A&AS* 80, 149
 Zinnecker H., Mc Caughrean M.J., Wilking B.A., 1993, In: Levy E.H., Lunine J.I. (eds.) *Protostars and Planets III*, University of Arizona Press, Tucson, p. 429
 Zinnecker H., Mc Caughrean M., Rayner J., 1997, In: Malbet F., Castets A. (eds.) *Low Mass Star Formation – from Infall to Outflow*. Poster proceedings of IAU Symp. 182, p. 198